A stress-controlled microfluidic shear viscometer based on smartphone imaging

Deepak E. Solomon, Amjad Abdel-Raziq & Siva A. Vanapalli

Rheologica Acta

ISSN 0035-4511

Rheol Acta
DOI 10.1007/s00397-016-0940-9

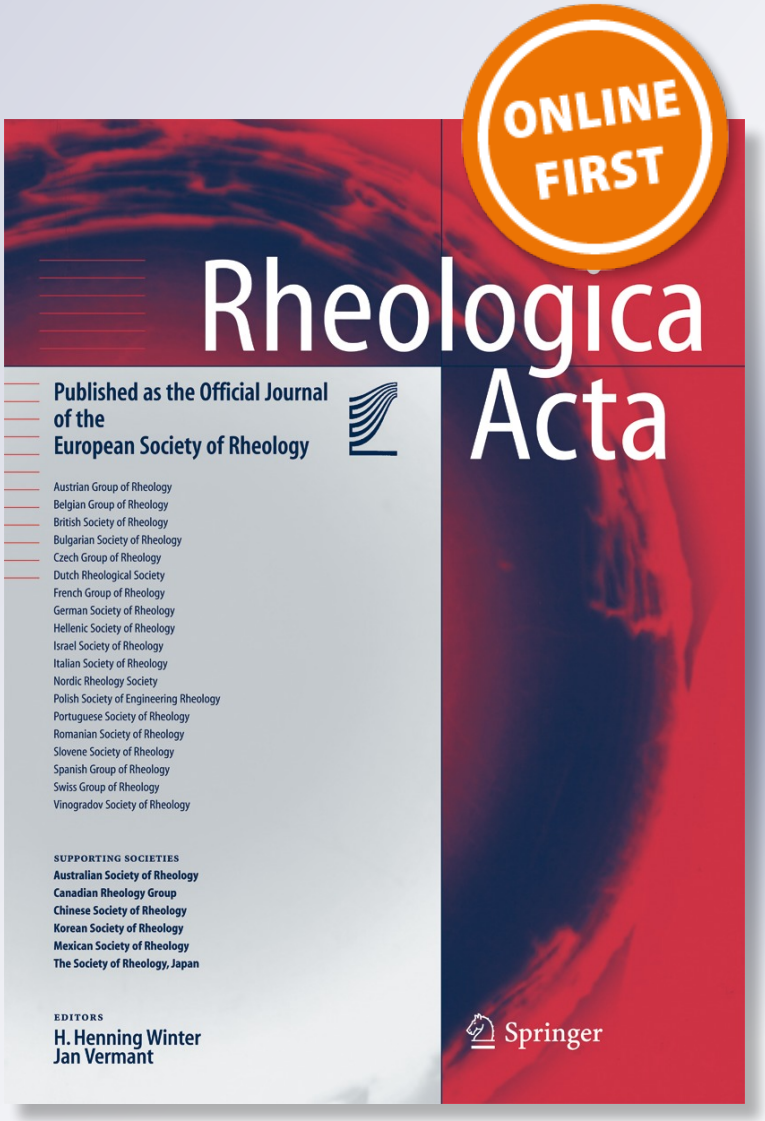

Springer

Your article is protected by copyright and all rights are held exclusively by Springer-Verlag Berlin Heidelberg. This e-offprint is for personal use only and shall not be self-archived in electronic repositories. If you wish to self-archive your article, please use the accepted manuscript version for posting on your own website. You may further deposit the accepted manuscript version in any repository, provided it is only made publicly available 12 months after official publication or later and provided acknowledgement is given to the original source of publication and a link is inserted to the published article on Springer's website. The link must be accompanied by the following text: "The final publication is available at link.springer.com".

Springer

Author's personal copy

Rheol Acta
DOI 10.1007/s00397-016-0940-9

ORIGINAL CONTRIBUTION

A stress-controlled microfluidic shear viscometer based on smartphone imaging

Deepak E. Solomon[1] · **Amjad Abdel-Raziq**[1] · **Siva A. Vanapalli**[1]

Received: 18 November 2015 / Revised: 26 March 2016 / Accepted: 21 April 2016
© Springer-Verlag Berlin Heidelberg 2016

Abstract We report a stress-controlled microfluidic shear viscometer with flow visualization aided by smartphone technology. The method involves driving the fluid into a microchannel at constant pressure and using the smartphone camera to track the fluid front in a glass capillary attached to the microchannel. We find that videos of interface propagation from the smartphone are of sufficient resolution that accurate pressure drop-flow rate relations can be determined to quantify the viscosity curves for complex fluids. We demonstrate that this simple 'iCapillary' device measures the shear viscosity of Newtonian and polymeric fluids over a broad range of shear rates (10–10,000 s^{-1}) that is in quantitative agreement with rotational rheometry. We further show that the simplicity of the iCapillary device allows for parallel analysis of viscosity of several samples. We performed multiplexed measurements of concentration dependence of high shear rate viscosity of globular protein solutions, and the results are in good agreement with models of suspension rheology as well as prior experimental data. Our approach is unique, since no on-chip sensing element is required other than the smartphone camera. This sensorless approach offers the potential to create inexpensive and disposable devices for point-of-care rheology of complex fluids and biological samples.

Keywords Microfluidics · Shear viscocity · Flow curve · Rheometer

✉ Siva A. Vanapalli
siva.vanapalli@ttu.edu

[1] Department of Chemical Engineering, Texas Tech University, Lubbock, TX 79409-3121, USA

Introduction

Shear viscometers are an important tool in characterizing the rheological properties of complex fluids for applications such as food processing (Rao 2007), consumer products (Buchmann 2001), pharmaceuticals (Purwar et al. 1988), inks, (Tabbernor 1988), polymers (Kontopoulou 2011), drilling fluids (Santoyo et al. 2001), lubricants (de Carvalho et al. 2010), and clinical diagnostics (Hurth et al. 2011). In many of these applications, it is desirable to quickly characterize the viscosity of one or more samples at the location where products are being made or processed, rather than being analyzed offsite. Macroscale rheometers although capable of performing a broad suite of precise rheological measurements are not well suited for onsite or point-of-care viscometry applications, because of their bulkiness and need for skilled operators. Furthermore, the capability of these devices to perform high-throughput measurements of multiple formulations is limited, making them more suitable for research laboratory settings rather than point-of-care testing. Viscosity measurement devices such as Saybolt, capillary tube, and rotational viscometers are more suited for onsite usage because of their non-complicated operation and cost effectiveness. Although handy, these devices have a number of limitations which include (i) the use of large sample volumes, (ii) cumbersome cleaning procedures if multiple sample measurements are needed, (iii) limited shear rate range, and (iv) the presence of non-viscometric flow kinematics (e.g., Saybolt viscometer) making it difficult to interpret viscosity data for complex fluids.

In the last decade, microfluidic shear viscometers (Galambos and Forster 1998; Lee and Tripathi 2005; Srivastava et al. 2005; Guillot et al. 2006; Pipe et al. 2008; Pan and Arratia 2012; Livak-Dahl et al. 2013) have emerged as alternative tools capable of addressing the above limitations

Published online: 01 June 2016

Author's personal copy

of conventional viscometers. Microfluidic viscometers developed to date use a variety of driving sources to introduce fluid flow in microchannels. In strain-rate controlled viscometers, constant fluid flow rate is imposed using syringe pumps (Guillot et al. 2006; Pipe et al. 2008; Pan and Arratia 2012; Guillot and Colin 2014; Solomon and Vanapalli 2014), while in stress-controlled viscometers a constant pressure drop is delivered using pressure sources (Livak-Dahl et al. 2013; Hudson et al. 2015) or capillary pressure (Srivastava et al. 2005; Han et al. 2007). Knowing the relation between pressure drop and flow rate, the viscosity of the fluid is determined. In these devices, depending on the driving force, the fluid response is measured using pressure sensors embedded on the channel surface (Pipe et al. 2008; Pan and Arratia 2012) or image-based detection of fluid interfaces (Lee and Tripathi 2005; Solomon and Vanapalli 2014; Guillot et al. 2006) or integrating a flow rate sensor (Hudson et al. 2015).

Despite several microfluidic shear viscometers being reported in the literature, current devices have some limitations. For example, in pressure-sensor-based viscometers, the sensing element is in contact with fluid flow, and this design may not be ideal for handling biological samples where use-and-throw capability is desired to avoid sample cross-contamination. Likewise, repeated handling of industrial-grade particulate fluids in these devices may become problematic due to adhesion of particles on channel and sensor surfaces, unless rigorous washing protocols are implemented. Finally, because pressure-sensor-based viscometers are flow-rate controlled, they do not scale favorably for parallelized analysis of samples.

Several microfluidic viscometers based on imaging have been developed (Lee and Tripathi 2005; Guillot et al. 2006; Livak-Dahl et al. 2013; Solomon and Vanapalli 2014). These image-based viscometry methods include those that rely on coflowing laminar streams (Lee and Tripathi 2005; Guillot et al. 2006; Solomon and Vanapalli 2014) or capillary imbibition of a fluid into a microchannel (Srivastava et al. 2005; Han et al. 2007). To determine sample viscosity, with co-flowing laminar streams interface width is measured, while interface motion is recorded during capillary imbibition. In contrast to on-chip sensor-based approaches, these devices have the advantage that there is no detection element present on the chip making the approach non-contact, however, these methods have some limitations. They require the use of research-grade microscopes and cameras to reliably detect the interface location, because of the microscale channel and interface width dimensions. Moreover, the co-flowing laminar stream approach might be problematic in measuring the viscosity of complex fluids that contain mutually miscible components and hydrodynamic instabilities might preclude precise control of the fluid-fluid interface location (Vanapalli et al. 2007; Cartas-Ayala and Karnik 2013; Solomon and Vanapalli 2014). Likewise, capillary imbibition viscometers require calibration chambers to determine capillary pressure and are sensitive to wetting defects.

In this work, we present a microfluidic viscometer that is simple and distinct from current image-based viscometers reported in the literature. It involves a microchannel where flow is driven using a constant pressure (or wall shear stress). The flow rate is determined by monitoring the slug (i.e., air–fluid interface) propagation in a millimeter-scale glass capillary connected to the microchannel (see Fig. 1). Because of the larger diameter glass capillary, we use the camera on a smartphone to record interface motion. We refer to this device as 'iCapillary'. Currently, smartphones contain cameras that are capable of recording images at 30 frames per second in 1024 pixels of vertical resolution (1024p). This video-recording capability provides significant opportunities for inexpensive visualization of fluid flows in microfluidic devices. Exploiting this imaging capability of consumer cameras, we show reliable measurement of viscosity curves for Newtonian and polymeric fluids. We also show that the high-shear rate viscosity of several different concentrations of protein solutions can be measured in parallel that may find potential applications in antibody-based therapeutics. Finally, we provide limits on operability of our iCapillary device.

Basic principle of viscosity measurement

Our method is based on quantifying pressure-drop versus flow rate relation for a given fluid, followed by determination of viscosity using the principles of slit-rheometry (Macosko 1994). A schematic of the device is shown in Fig. 1a. A constant pressure (P_c) is imposed at the inlet of a microchannel of width (w), height (h), and length (L_{ch}). The volumetric flow rate (Q) of the fluid in the microchannel is determined by measuring the mean velocity of the slug in the attached glass capillary using the in-built camera in the smartphone. The mean velocity of the slug is then multiplied by the cross-sectional area of the glass capillary to obtain the volumetric flow rate.

We now describe how the viscosity and shear rate for Newtonian and non-Newtonian fluids can be computed from experimental data. The foregoing analysis assumes that the dominant contribution to flow resistance comes from the microchannel and that $w >> h$ making the flow one-dimensional. Our devices are designed to ensure these assumptions are satisfied (see "iCapillary device design and operation" section).

The viscosity for a Newtonian fluid is given by,

$$\mu = \frac{\tau_w}{\dot{\gamma_0}} \tag{1}$$

where τ_w is the wall shear stress and $\dot{\gamma_0}$ is the apparent wall shear rate. The wall shear stress experienced by the microchannel in the iCapillary device is given by

$$\tau_w = \frac{(P_c - P_{h1} + P_L)wh}{2L_{ch}(w+h)} \tag{2}$$

Author's personal copy

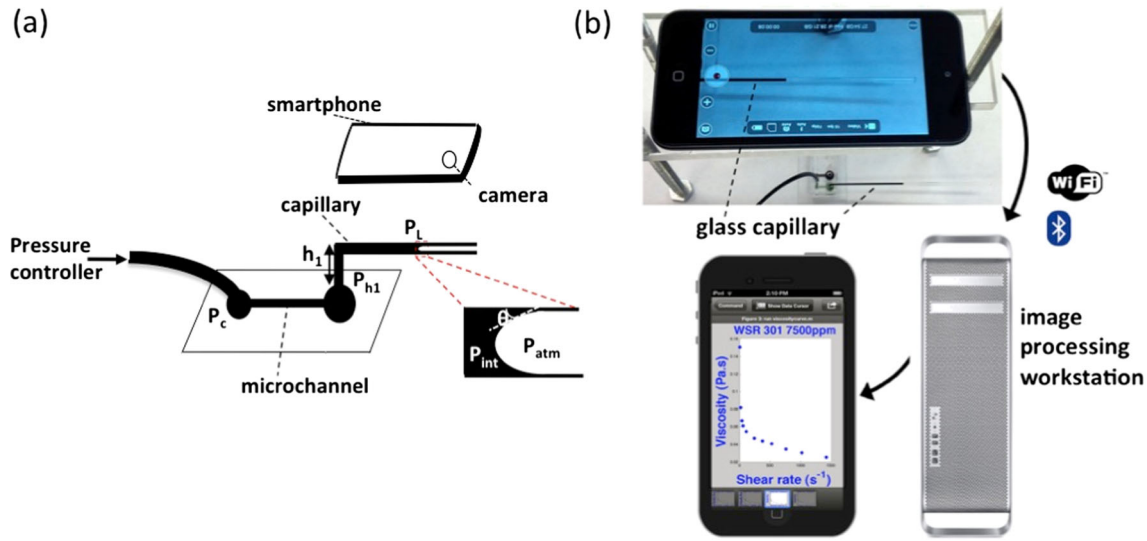

Fig. 1 Schematic and operation of the iCapillary-based viscometer. **a** The basic principle involves driving the fluid at a controlled inlet pressure and recording the motion of the air–fluid interface using the smartphone camera. The driving pressure from the controller is P_c, the static head due to the vertical section of capillary is P_{h1}. The inset shows the air–liquid meniscus where the Laplace pressure jump, $P_L = P_{atm} - P_{int}$. **b** Experimental set up showing the glass capillary connected to a microfluidic device. The smartphone resting on a custom-made three-leg stand with adjustable height is also shown. Our approach allows the ability to view the sample viscosity curve (computed offline) on the smartphone. In brief, the images are first captured using the smartphone followed by transferring the video files on a local Wi-Fi network to the image processing computer workstation. After the images are processed, the results are viewed on Matlab Mobile, which is installed on the smartphone

In Eq. (2), P_L is the Laplace pressure jump across the air–liquid interface and P_{h1} is the static head due to the short arm of the L-shaped glass capillary (see Fig. 1a). The derivation of Eq. (2) is provided in the Appendix.

For a Newtonian fluid, the apparent wall shear rate is

$$\dot{\gamma}_0 = \frac{6Q}{wh^2} \tag{3}$$

Both the wall shear stress and apparent wall shear rate can be determined from the microchannel geometry and known values of P_c, P_{h1}, P_L, and Q from experiments, enabling quantification of fluid viscosity.

For non-Newtonian fluids, the viscosity is still given by Eq. 1, except that the wall shear rate prescribed by Eq. 3 needs to be modified to account for the non-parabolic velocity profile which is characteristic of complex fluids. We use the Weissenberg-Rabinowitch Mooney analysis developed for a slit rheometer (Macosko 1994) and obtain the true wall shear rate and viscosity for the non-Newtonian fluid as,

$$\dot{\gamma} = \frac{\dot{\gamma}_0}{3}\left(2 + \frac{d(\ln\dot{\gamma}_0)}{d(\ln\tau_w)}\right) \tag{4}$$

Note that the term $\frac{d(\ln\dot{\gamma})}{d(\ln\tau_w)} = 1$ for Newtonian fluids and $\neq 1$ for non-Newtonian fluids, thereby accounting for the nonlinear relationship between shear rate and shear stress for non-Newtonian fluids. Eqs. (1–4) can thus be used to compute the viscosity versus shear rate curve for a non-Newtonian fluid. We calculate $d(\ln\dot{\gamma})/d(\ln\tau_w)$ by fitting a second order polynomial, which provides sufficient accuracy for the fluids used in this study.

iCapillary device design and operation

Device design

The microchannel was designed such that the flow is one-dimensional and entrance effects are negligible. The channel width is w = 1000 μm, height is $h \approx 31$ μm and length is L_{ch} = 0.473 cm. The aspect ratio of the microchannel, h/w = 0.031. In our study, the flow is assumed to be one-dimensional (1-D). The expression used to calculate shear rate (Eq.3) is strictly valid for 1-D flow, however, the equation to calculate wall shear stress (Eq. 2) does not necessitate the assumption of 1-D flow. To address how much error is introduced by using a 1-D assumption, we calculate the hydraulic resistance both from an exact solution of flow in a rectangular channel and that from an infinite parallel-plate (IPP) approximation [see Chapter 3 in Ref. (Bruss 2008) for the flow resistance equations]. At an aspect ratio of 0.031, the resistance is 3.2 % more than that calculated from the IPP approximation. Thus, our assumption of 1-D flow does not introduce significant errors in calculation of shear rates.

Author's personal copy

The entrance length (L_e) for laminar flows with Re < 2000 is given by (Pipe et al. 2008),

$$L_e = d_h\left(\frac{0.6}{1+0.035\mathrm{Re}} + 0.056\mathrm{Re}\right) \quad (5)$$

where Re is the Reynolds number and d_h is the hydraulic diameter of the microchannel. The maximum entrance length (corresponding to the highest shear rates attained in the device ~16,000 s^{-1}) is $L_e = 0.01L_{ch}$, justifying that the flow is fully developed in the microchannel.

The glass capillary was designed such that its flow resistance is negligible compared to the microchannel. The borosilicate glass capillary (BF-200, Sutter Instruments, CA) has an inner radius, $r = 0.76$ mm and is L-shaped (see Fig. 1a) with a short arm of length $h_1 \approx 5$ mm and a long arm of length, $L_{cap} = 8$ cm. The geometry of the capillary ensures <1 % contribution to the hydrodynamic resistance of the microchannel. The 5 mm length of the short arm is necessary for mechanical stability of the capillary while connecting to the microchannel. This length of the short arm corresponds to a hydrostatic head of $P_{h1} \approx 50$ Pa. For majority of the conditions used in this study, this static head contributes to <3 % of the driving pressure (P_c), nevertheless we accounted for this pressure loss in all of our calculations.

The capillary pressure due to the air–fluid interface was also designed to be small compared to the driving pressure by choosing a capillary of sufficiently large diameter. The capillary pressure (P_L) is given by

$$P_L = \frac{2\sigma\cos\theta}{r} \quad (6)$$

where σ is the surface tension between the fluid–air interface, θ is the contact angle between the fluid and the glass capillary (see inset of Fig. 1a). We estimated P_L from Eq. (6) using known values of surface tension of water–air interface at 20 °C (σ = 72.75 mN/m (Vargaftik et al. 1983)) and its contact angle with borosilicate glass (θ = 32°(Finlayson-Pitts et al. 2003)). For the glass capillary used in this study, $P_L \approx 160$ Pa. Note that as the glass is hydrophilic the shape of the interface is concave as shown in the inset of Fig. 1a, consistent with our observations. For the majority of conditions used in this work, capillary pressure contributes to <6 % to the driving pressure (P_c). Interfacially active molecules such as surfactants and proteins reduce air–water surface tension; therefore, we expect the contribution of P_L to be even lower in such cases. For simplicity, in all of our analysis, we used an upper bound of $P_L \approx 160$ Pa. In addition to reducing surface tension, surfactants and proteins can also form viscoelastic films at interfaces, which may affect our measurement technique. We address this potential concern in "Multiplexed viscosity measurements" section.

Device operation

The iCapillary device was tested with Newtonian (water-glycerol mixtures), polymeric fluids (polyethylene oxide, WSR-N60K, Dow Chemical Co., Midland, MI), and bovine serum albumin (BSA, Sigma Aldrich) solutions. Newtonian fluids and polymeric fluids were prepared as described previously (Solomon and Vanapalli 2014). The bovine serum albumin (BSA) solutions were prepared in 0.01 M phosphate buffered saline solution with concentrations varying from 5 to 250 mg/ml.

The device consists of a microfluidic channel fabricated using the soft lithography technique (Xia and Whitesides 1998). To fit the glass capillaries into the outlets of the PDMS microchannel, we punched holes slightly smaller than the external diameter of the glass capillary into the outlets of the PDMS microchannel. The capillaries were then pushed into the slightly smaller hole causing the elastic PDMS to expand and in turn form a leak proof seal. Additionally, we also ensured that the PDMS device was sufficiently thick (~3–5 mm) to prevent sagging of the capillaries that might cause fluid leakage. The glass capillaries were cleaned with ethanol, sonicated, and dried in an oven to ensure that dirt was not a factor in our experiments.

To generate viscosity curves different driving pressures were applied using an automated pressure controller (MCFS-flex, Fluigent, France). The reported accuracy of the pressure controllers is <1 % of the full scale. The motion of the fluidic slug was captured using a smartphone (iPod, Apple Inc., Cupertino, CA). To manipulate the frame rate and format for video capturing, we used a third party application (ProCAM, iTunes Store). The movies were recorded in mp4 file format at 15 frames per second. The calibration of the images was performed using a ruler, which yielded a pixel resolution of 100 μm/pixel. The images captured using the smartphone were transferred to an image processing workstation using a local Wi-Fi network. The transferred video files were then analyzed on the workstation using Matlab (Mathworks, Boston, MA). Typical size of the video files recorded range from 8 to 100 MB with data transfer rates of 1–2 Mbps. After the images are processed, the results are viewed on Matlab Mobile (which is installed on the iPod).

The image analysis was conducted on the image processing workstation using mostly Matlab (Mathworks, Boston, MA) (in limited cases Image J was also used). In instances where the fluidic slug moves <50 pixels (e.g., high fluid viscosity or low driving pressure), an automated algorithm was used to detect the location of the fluidic slug in the capillary. As shown in Fig. 2, the image is first cropped to have only the capillary in the field of view, a threshold is applied on the images, followed by *edge detect* to find the contours of the fluidic slug. Finally, a Hough transform is applied to the edges of the slug to determine the length of the fluidic slug. The error

Author's personal copy

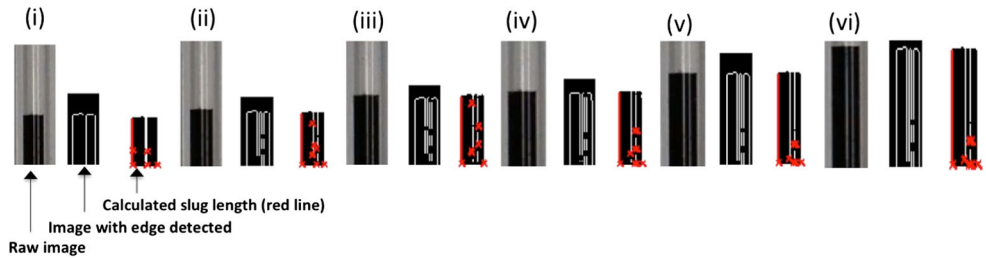

Fig. 2 Image processing steps involved in calculating the distance traveled by the fluidic slug over a period of time. Set of images at six different time steps (i)–(vi) are shown. The first image in each set represents the raw video image, the second image detects the processed contour of the fluidic slug and the third image identifies the slug length using Hough transform

in detecting the slug length is ±1 pixel. In instances where the fluidic slug moves >50 pixels, the Hough transform method was sub-optimal due to misalignment of the capillary with the edge of the image frame. In this case, the distance traveled by the fluidic slug was measured manually using Image J. The error in manually detecting the interface is ±3 pixels.

To obtain the mean fluid velocity of the slug, we record a video where the total distance traversed by the slug is at least 4 mm (or 40 pixels). We process the video and obtain distance versus time plots as shown in Fig. 3. We perform a linear fit to this data and obtain the mean velocity. It is evident from the figure that the distance versus time is always linear. To prevent startup issues, depending on the system condition (i.e., imposed pressure drop and fluid viscosity), we allow 2–7 s for the fluid to propagate into the horizontal portion of the capillary and allow an additional 5 s before video recording is initiated. Thus, about 10 s of start-up time is allowed before velocity calculations are initiated. We note that the shape variations of the interface are associated with typically 1 pixel fluctuation in interface position, which is minor compared to the 40 pixel traverse distance used to calculate mean fluid velocity of the slug. Finally, since the glass capillary is 80-mm long and is always in the field of view of the smartphone, we typically take about 10 data points per run, including some replicates if necessary.

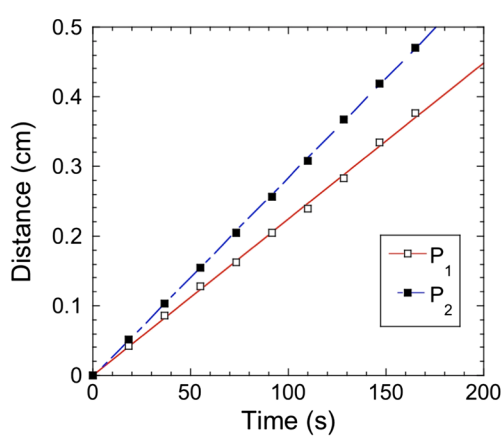

Fig. 3 Plot showing distance traveled by the fluidic slug over time at two imposed pressure drops for a Newtonian fluid (80 wt% glycerol solution). The *lines* represent linear fits to the data

All the viscosity data determined from the iCapillary were compared with a mechanical rheometer (AR2000, TA Instruments, New Castle, DE). A cone-and-plate fixture was used for mechanical rheometry. The tolerance for all rheometer measurements in the study was set to be <5 %. Both the microfluidic and rheometer experiments were conducted at a temperature of 22 ± 1 °C.

Results and discussion

Single iCapillary device

To assess the capability of the iCapillary device for measuring viscosity, we first tested Newtonian fluids. We chose five different glycerol solutions having a viscosity range between ~20–200 mPa-s. The viscosity values obtained from the iCapillary for the five different fluids were compared with the data obtained from a mechanical rheometer. As shown in Fig. 4, the iCapillary data is in good agreement with that from the rheometer. Each data point in Fig. 4 is a mean viscosity computed from at least five different shear rates ranging between ~10 and 1000 s^{-1}. The inset of Fig. 4 shows the viscosity data as a function of shear rate for a 20 mPa-s glycerol solution that is consistent with the rheometer value. However, for $\dot{\gamma} > \sim 2000\ s^{-1}$ the viscosity obtained from the iCapillary device deviates significantly (~30 %) due to the expansion of the elastomeric microchannel at high pressure drops. Opportunities however exist to reliably access viscosity data even at higher shear rates by employing non-deformable microchannels (see further discussion in "Limits of operability of the iCapillary device" section).

Next, we determined the capability of the iCapillary to measure the viscosity of polymeric fluids having a shear-rate dependent viscosity. We chose polyethylene oxide (PEO) fluids having an approximate molecular weight of 2×10^6 g/mol (Vanapalli et al. 2005) as our model fluid. Two different concentrations of 1 and 2 wt% were tested. Figure 5 shows the measured viscosities of these polymeric fluids as a function of shear rate using the iCapillary device and their comparison with viscosities obtained from the mechanical rheometer. The data agrees well with the iCapillary device, indicating the capability of our method to

Author's personal copy

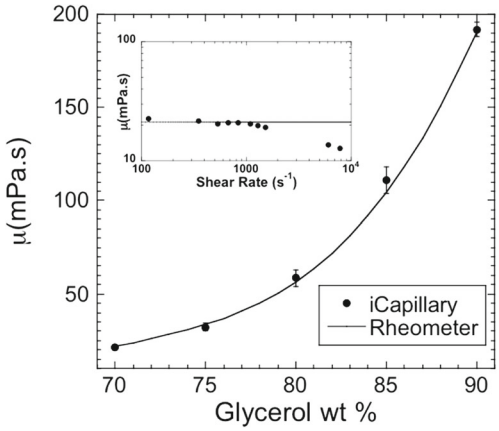

Fig. 4 Viscosity measured from the iCapillary (symbols) for Newtonian glycerol solutions compared with that from a mechanical rheometer. The error bar comes from averaging viscosity values from at least five different shear rates. Inset shows viscosity of 70 wt% glycerol as a function of shear rate (*symbols*) compared with the mean value obtained from the rheometer (drawn as a *line*). The data deviates at high shear rates due to elastic deformation of the PDMS microchannel

record viscosity curves for non-Newtonian fluids over a broad range of shear rates (10–10,000 s^{-1}).

Multiplexed viscosity measurements

The simplicity of our approach involving a microchannel and a connected glass capillary also allows parallelized measurements of viscosity of multiple samples. As shown in Fig. 6, several glass capillaries can be connected to a single-molded device containing multiple microchannels, enabling multiplexed viscometry. Here, we demonstrate two formats for multiplexed viscometry. For Newtonian fluids, the viscosity of several samples can be measured by comparing to a reference fluid of known viscosity. This comparative viscometry method not only simplifies the data analysis on multiple samples but also might be practically relevant for applications

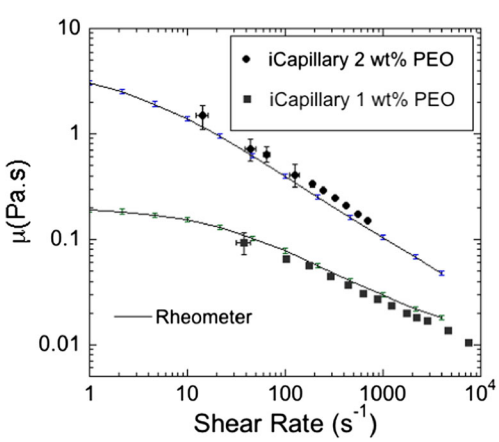

Fig. 5 Viscosity values of 2 wt% (*circles*) and 1 wt% (*squares*) concentrations of PEO solution obtained using the iCapillary. The *curves* are data from a rotational rheometer, with 5 % error bars on individual data points

involving Newtonian fluids such as lubricants (Bair et al. 2001) and ionic liquids (Yu et al. 2012).

For non-Newtonian fluids, a straightforward extension of the single iCapillary device (c.f. "Single iCapillary device" section) to multiple samples can be used. Here, a single video recording can be taken for several samples flowing through a set of capillaries for a specified length of time. The resulting images can be analyzed for each of the capillaries and a viscosity curve can be generated for each sample. As one demonstrative application of this multiplexed viscometry, we measure concentration-dependent viscosity of protein solutions which is important in subcutaneous injection of antibody-based therapeutics where both the dose and syringeability need to be optimized (Burckbuchler et al. 2010; Allmendinger et al. 2014). We discuss both these routes to multiplexed viscometry using the iCapillary approach in the next two sections.

Comparative microfluidic viscometry for Newtonian fluids

Comparative viscometry can be easily implemented on the iCapillary device because if the applied pressure drop and channel dimensions are the same, and the two fluids are tracked for the same duration, the ratio of viscosities between the reference and 'test' fluids is then inversely proportional to the ratio of their distance (d) traversed, i.e.,

$$\frac{\mu_1}{\mu_2} = \frac{d_2}{d_1} \tag{7}$$

Eq. (7) is valid only for Newtonian fluids because different non-Newtonian fluids may have different values of $\frac{d(\ln\dot{\gamma})}{d(\ln\tau_w)}$ Since Eq. (7) holds for any driving pressure, the comparative method provides the flexibility to choose the appropriate driving pressure depending on the fluid viscosity. In addition, if needed, the shear rate experienced by the Newtonian test fluid can be calculated knowing the shear rate of the reference fluid since

$$\frac{\dot{\gamma}_1}{\dot{\gamma}_2} = \frac{d_1}{d_2} \tag{8}$$

We demonstrate comparative viscometry by taking four Newtonian fluids in the viscosity range of 35–150 mPa-s. We select the fluid with viscosity of μ_{ref} = 35 mPa-s as the reference sample and determine the viscosity of the other three fluids from the iCapillary device by comparing the relative distances moved by the respective fluidic slugs. As shown in Fig. 6a, the fluids are brought to the same interface location by applying the same driving pressure and adjusting the duration of applied pressure. When the pressure is applied for an additional duration of Δt = 10 s, as expected, we observe high viscosity fluids move less than the low viscosity fluids (see Fig. 6b). Visual inspection of the images allows one to quickly

Author's personal copy

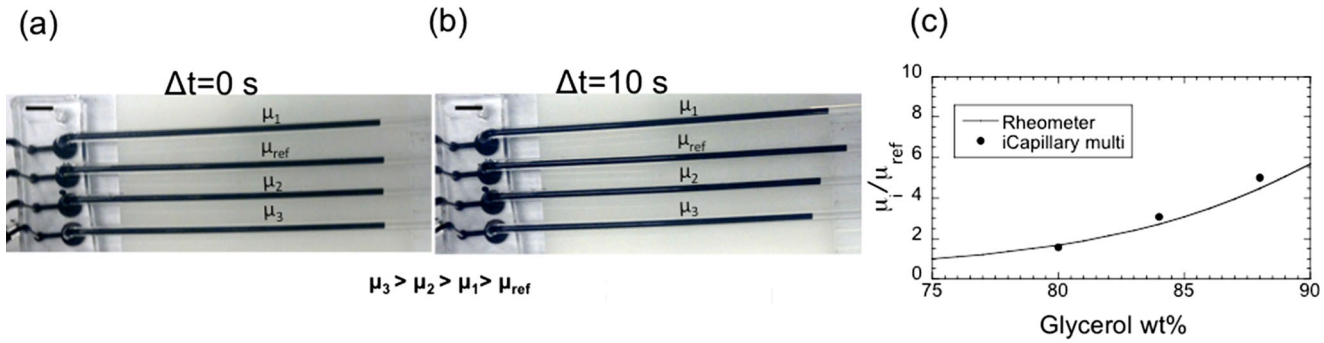

Fig. 6 Comparative microfluidic viscometry for parallel analysis of fluids. **a** Image showing the setup for the multiplexed experiments where all the different fluids have been brought to the same interface location. **b** Image showing that after a duration Δt = 10 s, high viscosity fluids travel less distance than low viscosity fluids. **c** Relative viscosities obtained from the iCapillary using the multiplexed method compared with those obtained from the rheometer

rank the viscosity of the four different fluids. In Fig. 6c, we quantify the results obtained from the comparative method against the rheometer and find good agreement. We note that to illustrate the comparative viscometry principle, the interface location for different fluids was adjusted to be the same in Fig. 6a, although this is not required.

Concentration dependent viscosity of protein solutions

In this section, we demonstrate that parallel analysis of protein solutions can be accomplished using the iCapillary device. We use bovine serum albumin as a model for monoclonal antibodies. Antibody-based therapies are being increasingly used for diseases in which the immune system is compromised (Goswami et al. 2013). In antibody-based therapeutics, it is desirable to deliver a high dose for effective therapy (Shire et al. 2004). However, high dosage necessarily leads to increased solution viscosity, which might adversely affect their needle-based injection for subcutaneous applications (Burckbuchler et al. 2010; Allmendinger et al. 2014). Thus, during formulation of antibody-based therapeutics, it is critical to optimize both dosage and solution viscosity.

To demonstrate the suitability of our method for measuring the effect of dosage on protein solution viscosity (μ_p), we measured the viscosity of BSA solutions at eight different concentrations (5–250 mg/ml), in the shear rate range of 1400–16,000 s^{-1}. This shear rate range is commensurate with the shear rates experienced by protein solutions when injected using 26- and 30-G syringe needles (Burckbuchler et al. 2010). In this range of shear rates, BSA solutions behave as Newtonian fluids (Sharma et al. 2011).

Figure 7a shows the capillaries that are loaded with different concentrations of BSA solutions. The air–fluid interface is clearly visible allowing us to record the slug velocity without any added marker dyes. Figure 7b shows the values of relative viscosity (μ_p/μ_o) of BSA solutions as a function of the protein volume fraction (ϕ). Here, μ_o is the solvent viscosity. We calculate the volume fraction of the protein solution, $\phi = 4\pi c N_A a^3/3M_w$, where c is the concentration of the BSA solution, a = 3.48 nm is the hydrodynamic radius (Ikeda and Nishinari 2000) and M_w = 66.5 kDa is the molecular weight of BSA (Peters 1996) and N_A is the Avogadro number. We find a small increase in solution viscosity for $\phi < 0.1$, after which there is a rapid increase in the viscosity.

A potential concern with viscosity measurement using the iCapillary is the presence of the air–liquid interface, which has been shown to yield ambiguous viscosity data due to the formation of viscoelastic protein films (Sharma et al. 2011). To address this issue, we first compared predictions from suspension rheology (Mewis and Wagner 2012). For a suspension of rigid spheres, the relative viscosity as calculated by Batchelor and Green (BG) (Batchelor and Green 1972) is given by,

$$\frac{\mu_p}{\mu_0} = \left(1 + \lambda\phi + \lambda_1\phi^2 + O\left[\phi^3\right]\right) \tag{9}$$

where $\lambda = 2.5$ is the contribution to solution viscosity from an isolated particle and $\lambda_1 = 6.2$ represents the hydrodynamic contribution due to pair-wise hard-sphere interactions. As shown in Fig. 7b, the BG model fits the experimental data well up to a volume fraction of ~0.1. We also tested the semi-empirical Kreiger Dougherty (Krieger and Dougherty 1959) (KD) model given by,

$$\frac{\mu_p}{\mu_0} = \left(1 - \frac{\phi}{\phi_m}\right)^{-[\mu]_1\phi_m} \tag{10}$$

It has been shown that the Kreiger-Dougherty (KD) model is successful in predicting the viscosity increase for suspensions with packing fractions as high as 0.63 (Genovese et al. 2007). In Eq. 10, ϕ_m is the maximum packing fraction and for rigid spheres in shear flow, $\phi_m = 0.7$ (Brownsey et al. 2003) and first-order intrinsic viscosity ($[\mu]_1$) is taken as 2.5 (Mueller et al. 2009; Dörr et al. 2013). Using these two parameter values, we find good agreement of the KD model with our iCapillary data.

The above analysis shows that the hard-sphere rheology models appear to fit our iCapillary data reasonably well indicating

Author's personal copy

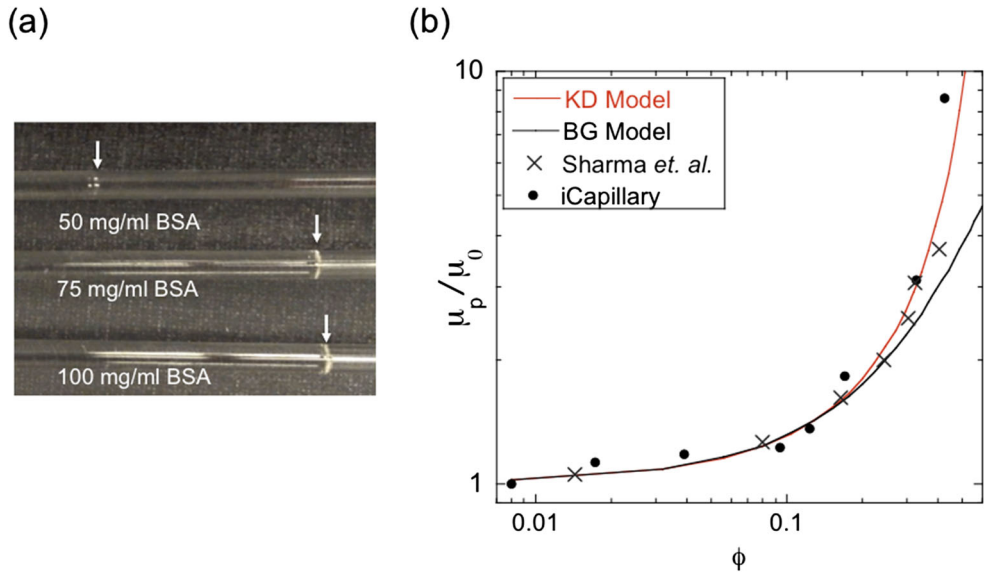

Fig. 7 Multiplexed iCapillary for viscosity measurements of protein solutions. **a** Image showing capillary loaded BSA solutions at three different concentrations at the same applied pressure drop. The *arrows* indicate the location of the fluid interface. **b** The relative viscosity as a function of volume fraction of BSA obtained from the iCapillary and compared with models of suspension rheology (KD—Krieger Dougherty and BG—Batchelor Green). Also shown is the data reproduced from Sharma et al. (2011) where a microfluidic viscometer embedded with pressure sensors (VROC, Rheosense Inc., CA) was used to measure the viscosity of BSA solutions

that BSA can be modeled as a colloidal sphere. However, a recent study suggests that the assumption that BSA is a hard sphere may be incorrect (Sarangapani et al. 2015). Therefore, to further address the issue of interfacial viscoelastic films, we also compared the viscosity data produced from the iCapillary with that from Sharma et al. (Sharma et al. 2011), where a microfluidic slit viscometer (VROC, Rheosense Inc., CA) that is devoid of interfacial effects was used to measure the viscosity of BSA solutions. As shown in Fig. 7b, the results match well further affirming the absence of interfacial viscoelastic effects in our method. Thus, our iCapillary device is capable of measuring quantitatively the viscosity of protein solutions in a parallelized manner, without issues of viscoelastic skin formation at the air–liquid interface.

The reason that viscoelastic skin formation does not contaminate our viscosity data is probably because (i) the surface area occupied by the interface is much smaller in the iCapillary device compared to a rotational rheometer (for example, cone and plate) making the contribution of interfacial viscoelastic stress much smaller than the applied stress in the iCapillary and (ii) the air–liquid interface in the capillary moves continuously during the measurement, potentially disrupting any formation of viscoelastic films that typically form on the time-scales of several minutes (Sharma et al. 2011).

Limits of operability of the iCapillary device

In this section, we discuss the errors and operating limits of our iCapillary device in relation to viscosity and shear rates than can be achieved with our technique.

Errors in measurement of fluid viscosity and shear rate

In this study, we find that the error in measured viscosity is typically ~5 % for water-like fluids at high shear rates. When high viscosity fluids are used, the error is larger, ~15 % at lower shear rates because of the small distance moved by the fluidic slug. For example, a non-Newtonian fluid that has a viscosity of 10 Pa-s at 10 s^{-1} will move 5 pixels in 10 min. The larger error for high viscosity fluids could be reduced by using a longer video acquisition time, but this may necessitate more consumption of memory on the camera.

Bounds on viscosity and shear rate

To determine the operating window for the iCapillary in terms of viscosity and shear rate, we recognize from Eqs. (1) and (2) that

$$\mu\dot{\gamma} = \frac{(P_c - P_{h1} + P_L)wh}{2L_{ch}(w+h)} \tag{11}$$

When the applied pressure from the controller, $P_c = 0$, then the viscosity-shear rates obtainable are set purely by surface tension assuming negligible hydrostatic pressure contribution. Using Eq. (11), in Fig. 8, we show this surface-tension dominated regime for $P_L = 0.16$ kPa and for the microchannel geometry used in this study. When $P_c >> P_L$, then the viscosity-shear rate regime is dominated by the applied pressure. To illustrate this regime in Fig. 8, we have drawn two curves, one of which corresponds to

Author's personal copy

$P_c = 10$ and $P_L = 1.6$ kPa and the other corresponds to $P_c = 30$ kPa, where significant elastic deformation of the microchannel is present. Thus, the shaded region in Fig. 8 corresponds to the operation of our PDMS-based iCapillary device.

The upper limit on the viscosity and shear rate that can be achieved in our PDMS devices is dictated by the maximum sustainable pressure drop, before appreciable changes in channel cross-section occur. An estimate of the fractional deviation in flow rate ($\Delta Q/Q$) due to change in channel height can be obtained by balancing the pressure and elastic stresses giving rise to (Gervais et al. 2006),

$$\frac{\Delta Q}{Q} \sim \frac{3c_1 \Delta PW}{2Eh_0} \tag{12}$$

where ΔP is the pressure drop across the microchannel, w is the width of the channel, c_1 is a proportionality constant taken as 0.33 (Gervais et al. 2006) and E (=2.2 MPa) is the elastic modulus of PDMS. When operating our device at ΔP = 30 kPa, based on Eq. (18), we expect the flow rate to increase by 20 % producing a corresponding reduction in estimated viscosity. This deviation is roughly consistent with the departure reported in the inset of Fig. 4a, where the highest pressure drop imposed was 30 kPa. We used this applied pressure to identify the operation window for the iCapillary device in Fig. 8.

In this study, we demonstrated that shear rates as high as ~10^4 s^{-1} can be achieved (see Fig. 5). By making the devices in non-deformable channels, the shear rate can be further increased. Ultimately, the highest accessible shear rate is limited by the maximum frame rate (30 frames/s) of the smartphone that restricts the maximum slug velocity that can be measured. For water-like fluids, we estimate that the maximum shear rate is around ~40,000 s^{-1}. With the advent of new smartphone technology, it is possible that much higher shear rates can be accessed.

The lowest accessible shear rate is determined by the minimum driving pressure that can be reliably delivered to the channel. In our setup, the minimum driving pressure is $P_c = 0.5$ kPa. For water-like fluids, this corresponds to a shear rate of 1640 s^{-1}. For fluids of very high viscosity, the driving pressure is not necessarily limiting in non-deformable microchannels, but the experiments can be time consuming. For example for a fluid that is 1000 times more viscous than water, to obtain accurate viscosity measurements (fluidic slug must move a minimum of 20 pixels) at shear rates <10 s^{-1}, about 40 min of imaging is needed.

In this study, we tested only aqueous fluids due to the good compatibility of PDMS devices to aqueous solutions. It is possible to configure the method for non-aqueous fluids by changing the material of the microfluidic device. An additional limitation of our method could be that for complex fluids containing suspensions and emulsions, particle size, and affinity to channel and capillary walls may present some measurement issues.

Comparison of iCapillary device with other image-based microfluidic viscometers

In this section, we discuss other image-based microfluidic viscometers and contrast their capabilities with respect to the iCapillary device.

Prior image-based viscometry methods include those that rely on co-flowing laminar streams (Lee and Tripathi 2005; Guillot et al. 2006; Solomon and Vanapalli 2014) or capillary imbibition (Srivastava et al. 2005; Han et al. 2007) of a fluid into a microchannel. To determine sample viscosity, with co-flowing laminar streams interface width is recorded, while interface motion is recorded during capillary imbibition. Although sensorless, these methods require use of research-grade microscopes and cameras to reliably detect the interface

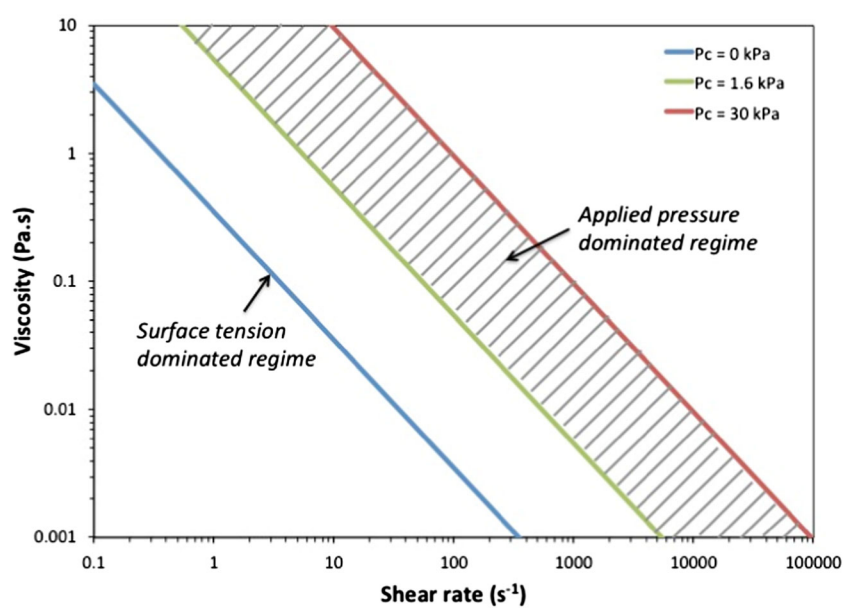

Fig. 8 Operating window for the iCapillary device used in this study. The diagram shows the surface tension dominated regime ($P_c = 0$) as well as the applied pressure dominated regime where $P_c \neq 0$

Author's personal copy

location, because of the microscale channel and interface width dimensions, making them more suitable for laboratory environments. Moreover, the co-flowing laminar stream approach might be problematic in measuring the viscosity of complex fluids that contain mutually miscible components and hydrodynamic instabilities might preclude precise control of the fluid–fluid interface location (Vanapalli et al. 2007; Cartas-Ayala and Karnik 2013; Solomon and Vanapalli 2014).

Due to the interface motion in a conduit, our approach resembles microfluidic capillary viscometers (μCVs) (Srivastava et al. 2005; Han et al. 2007) where capillary pressure is used to drive fluid flow rather than applied pressure. Both the μCVs and the iCapillary device allow use-and-throw capability, with the μCVs needing much smaller fluid sample volume (typically 1–10 μl). Nevertheless, the iCapillary device has a number of distinct features that offer significant benefits. (i) In μCVs, the pressure drop is generated by the capillary pressure and therefore needs to be estimated through a calibration chamber (Srivastava et al. 2005). In our device, pressure drop is known and can be varied over a broad range. (ii) The maximum pressure drop in a μCV is determined by the wettability characteristics and geometry of the microchannel making the technique best suited for low-viscosity fluids and low shear rates (10–1000 s^{-1}). In the iCapillary device, the pressure drop is tunable allowing characterization of both high and low viscosity fluids over a much broader range of shear rates (10–10,000 s^{-1}).

Conclusions

In this work, we show a smartphone-based microfluidic viscometer, which is capable of quantifying the viscosity curves for both Newtonian and non-Newtonian fluids. To collect viscosity data over a shear rate range of ~10–10,000 s^{-1} currently requires about 1 mL of sample, 20 min of experimentation time and another 40 min of off-line data analysis. This throughput is comparable to conventional rheometers.

However, unlike conventional rheometers, which serially process samples, we demonstrate that the iCapillary device can process samples in parallel. In this case, the iCapillary device is likely to outperform the rheometer since all the samples can be delivered using a single pressure source, and because several capillaries are captured on an image, only a single video file need to be processed for quantifying viscosity of multiple samples.

The number of samples that can be tested simultaneously is only be limited by the field of view of the camera in the smart phone. For the smartphone used in this study, we estimate that it can simultaneously image ~30 capillaries. Thus, our simple method has the potential to determine viscosity curves for a large number of samples in parallel, profoundly saving time and manpower.

The basic platform demonstrated here could be further improved. Specific 'apps' can be designed that will allow image and data analysis on the smartphone itself, rather than transferring files to be analyzed offline. Both the microchannel and glass capillary can be fabricated as a single unit using technologies such as 3D printing. With these additional improvements, our device can find significant potential for onsite shear viscometry as well as in applications that desire disposable devices.

Finally, in this work, we used a straight microchannel and focused on shear viscometry. However, our approach can be expanded to other microfluidic geometries including a hyperbolic contraction for measurement of apparent extensional viscosity of complex fluids (Galindo-Rosales et al. 2013).

Acknowledgments We thank William S. Wang and Biddut Bhattacharjee for useful discussions and Prof. Rajesh Khare for access to the rheometer. We acknowledge the donors of the American Chemical Society–Petroleum Research Fund (Grant No. 50521-DNI9) for partial support of this work.

Compliance with ethical standards

Conflict of interest This technology has been licensed to Neofluidics LLC. Deepak Solomon is an equity holder and employee of Neofluidics LLC. Deepak Solomon and Siva Vanapalli qualify to receive royalty distributions from patents assigned to Texas Tech University and licensed for commercial development to Neofluidics LLC.

Appendix

Wall shear stress relation for the microchannel in the iCapillary device

To calculate the viscosity for a Newtonian fluid, we use a resistive network approach similar to electrical circuits, where the relation between pressure drop and flow rate is specified using the analogy of Ohm's law. A schematic representation of the iCapillary device is shown in Fig. 9, which also depicts the pressures at different sections of the device. The pressure drop of a fluid flowing through a conduit can be determined from the product of the hydrodynamic resistance of the fluid (R) and the volumetric flow rate (Q). The hydrodynamic resistance is a function of fluid viscosity and conduit dimensions.

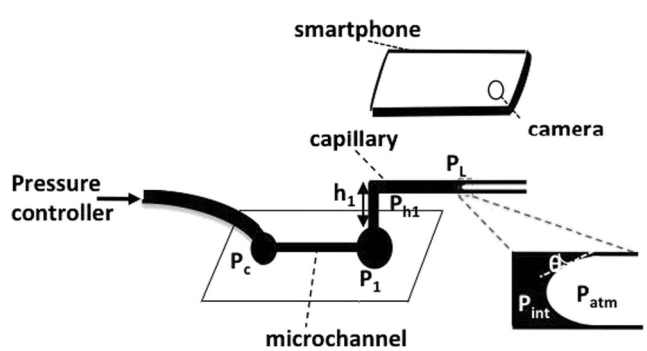

Fig. 9 A schematic diagram of the iCapillary device. The top right illustration shows the magnified view of the air-fluid interface having a contact angle, q, with the wettable surface (i.e. glass capillary in our experiment)

Author's personal copy

For the microchannel, the pressure drop and flow rate relation is given by

$$P_c - P_1 = QR_c \tag{1}$$

where P_c, P_1 and R_c are the inlet pressure, outlet pressure and hydraulic resistance of the microchannel respectively.

Likewise for the glass capillary, the pressure drop and flow rate relation is given by

$$P_1 - P_{int} = P_{h1} + QR_g \tag{2}$$

where P_{int}, P_{h1} and R_g are the internal pressure, hydrostatic head and the hydraulic resistance of the glass capillary respectively.

Finally, the Laplace pressure jump (P_L) across the air-water interface is given by

$$P_{atm} - P_{int} = P_L \tag{3}$$

where P_{atm} is the atmospheric pressure, taken as zero.

From Eqs. (1) – (3), we get

$$P_c + P_L - P_{h1} = Q\left(R_g + R_c\right) \tag{4}$$

Since $R_g << R_c$, we obtain the pressure drop across the microchannel (ΔP) as

$$\Delta P = QR_c = P_c + P_L - P_{h1} \tag{5}$$

Taking a control volume inside the microchannel and balancing the forces due to pressure and wall shear stress gives

$$\tau_w[2L_{ch}(w+h)] = \Delta P(wh) \tag{6}$$

In Eq. (6), L_{ch}, w and h are the length, width and height of the microchannel respectively. Using Eq. (5) in Eq. (6), we thus obtain the wall shear stress experienced by the microchannel in the iCapillary device as

$$\tau_w = \frac{(P_c - P_{h1} + P_L)wh}{2L_{ch}(w+h)} \tag{7}$$

References

Allmendinger A, Fischer S, Huwyler B, Mahler HC, Schwarb E, Zarraga IE, Mueller R (2014) Rheological characterization and injection forces of concentrated protein formulations: an alternative predictive model for non-Newtonian solutions. Eur J Pharm Biopharm 87(2): 318–328

Bair S, Jarzynski J, Winer WO (2001) The temperature, pressure and time dependence of lubricant viscosity. Tribol Int 34(7):461–468

Batchelor GK, Green JT (1972) The hydrodynamic interaction of two small freely-moving spheres in a linear flow field. J Fluid Mech 56(2):375–400

Brownsey GJ, Noel TR, Parker R, Ring SG (2003) The glass transition behavior of the globular protein bovine serum albumin. Biophys J 85(6):3943–3950

Bruss H (2008) Theoretical microfluidics. Oxford University Press, Oxford

Buchmann, S. (2001). Main cosmetic vehicles. Handbook of Cosmetic Science and Technology. A. O. Barel, M. Paye and H. I. Maibach. New York, Marcel Dekker, Inc.: 145–171.

Burckbuchler V, Mekhloufi G, Giteau AP, Grossiord JL, Huille S, Agnely F (2010) Rheological and syringeability properties of highly concentrated human polyclonal immunoglobulin solutions. Eur J Pharm Biopharm 76(3):351–356

Cartas-Ayala M, Karnik R (2013) Time limitations and geometrical parameters in the design of microfluidic comparators. Microfluid Nanofluid 17(2):359–373

de Carvalho MJS, Seidl PR, Belchior CRP, Sodre JR (2010) Lubricant viscosity and viscosity improver additive effects on diesel fuel economy. Tribol Int 43(12):2298–2302

Dörr A, Sadiki A, Mehdizadeh A (2013) A discrete model for the apparent viscosity of polydisperse suspensions including maximum packing fraction. Journal of Rheology (1978-present) 57(3):743–765

Finlayson-Pitts BJ, Wingen LM, Sumner AL, Syomin D, Ramazan KA (2003) The heterogeneous hydrolysis of NO2 in laboratory systems and in outdoor and indoor atmospheres: an integrated mechanism. Phys Chem Chem Phys 5(2):223–242

Galambos P, Forster F (1998) An Optical Microfluidic Viscosmeter. ASME Int. Mech.Eng.Cong.&Exp 66:187–191

Galindo-Rosales FJ, Alves MA, Oliveira MSN (2013) Microdevices for extensional rheometry of low viscosity elastic liquids: a review. Microfluid Nanofluid 14:1–19

Genovese DB, Lozano JE, Rao MA (2007) The rheology of colloidal and Noncolloidal food dispersions. J Food Sci 72(2):R11–R20

Gervais T, El-Ali J, Gunther A, Jensen KF (2006) Flow-induced deformation of shallow microfluidic channels. Lab Chip 6(4):500–507

Goswami S, Wang W, Arakawa T, Ohtake S (2013) Developments and challenges for mAb-based therapeutics. Antibodies 2:452–500

Guillot P, Colin A (2014) Determination of the flow curve of complex fluids using the Rabinowitsch- Mooney equation in sensorless microrheometer. Microfluid. Nanofluid. 17:605–611

Guillot P, Pascal P, Salmo JB, Mathieu B, Colin A (2006) Viscosimeter on a microfluidic chip. Langmuir 22:6438–6445

Han Z, Tang X, Zheng B (2007) A PDMS viscometer for microliter Newtonian fluid. J Micromech Microeng 17(9):1828–1834

Hudson SD, Sarangapani P, Pathak JA, Migler KB (2015) A microliter capillary rheometer for characterization of protein solutions. J Pharm Sci 104(2):678–685

Hurth C, Klein K, van Nimwegen L, Korn R, Vijayaraghavan K, Zenhausern F (2011) Clinical diagnostic of pleural effusions using a high-speed viscosity measurement method. J Appl Phys 110(3)

Ikeda S, Nishinari K (2000) Intermolecular forces in bovine serum albumin solutions exhibiting solid-like mechanical behaviors. Biomacromolecules 1(4):757–763

Kontopoulou M (2011) Applied polymer rheology:polymeric fluids with industrial applications. Wiley, New York

Krieger IM, Dougherty TJ (1959) A mechanism for non-Newtonian flow in suspensions of rigid spheres. Transactions of The Society of Rheology (1957–1977) 3(1):137–152

Lee J, Tripathi A (2005) Intrinsic viscosity of polymers and biopolymers measured by microchip. Anal Chem 77(22):7137–7147

Livak-Dahl E, Lee J, Burns MA (2013) Nanoliter droplet viscometer with additive free operation. Lab Chip 13(2):297–301

Macosko CW (1994) Rheology: principles, measurements and applications. Wiley-VCH, New York

Mewis J, Wagner NJ (2012) Colloidal suspension rheology. Cambridge University Press, Cambridge

Mueller S, Llewellin E, Mader H (2009) The rheology of suspensions of solid particles. Proceedings of the Royal Society of. London A, Mathematical, Physical and Engineering Sciences, The Royal Society

Pan, L. and P. E. Arratia (2012). A high-shear, low Reynolds number microfluidic rheometer. Microfluidics and Nanofluidics(1613–4982).

Peters T (1996) All about albumin: biochemistry, genetics, and medical applications. Academic Press, San Diego

Author's personal copy

Pipe CJ, Majmudar TS, McKinley GH (2008) High shear rate viscometry. Rheol Acta 47:621–642

Purwar S, Lim JK, Mauger JW, Howard SA (1988) Measuring viscosity of pharmaceutical and cosmetic semisolids using normal stress. J Soc Cosmet Chem 39(4):241–258

Rao MA (2007) Rheology of fluid and semisolid foods: principles and applications. Springer, New York

Santoyo E, Santoyo-Gutierrez S, Garcia A, Espinosa G, Moya SL (2001) Rheological property measurement of drilling fluids used in geothermal wells. Appl Therm Eng 21:283–302

Sarangapani PS, Hudson SD, Jones RL, Douglas JF, Pathak JA (2015) Critical examination of the colloidal particle model of globular proteins. Biophys J 108(3):724–737

Sharma V, Jaishankar A, Wang YC, McKinley GH (2011) Rheology of globular proteins: apparent yield stress, high shear rate viscosity and interfacial viscoelasticity of bovine serum albumin solutions. Soft Matter 7(11):5150–5160

Shire SJ, Shahrokh Z, Liu J (2004) Challenges in the development of high protein concentration formulations. J Pharm Sci 93(6):1390–1402

Solomon D, Vanapalli S (2014) Multiplexed microfluidic viscometer for high-throughput complex fluid rheology. Microfluid Nanofluid 16(4):677–690

Srivastava N, Davenport RD, Burns MA (2005) Nanoliter viscometer for analyzing blood plasma and other liquid samples. Anal Chem 77: 383–392

Tabbernor, A. (1988). Rheology of printing inks. The Printing Ink Manual. R. H. Leach, C. Armstrong, J. F. Brown et al. US, Springer: 666–698.

Vanapalli SA, Islam MT, Solomon MJ (2005) Scission-induced bounds on maximum polymer drag reduction in turbulent flow. Physics of Fluids, 17(9):095108

Vanapalli SA, van den Ende D, Duits MHG, Mugele F (2007) Scaling of interface displacement in a microfluidic comparator. Appl Phys Lett 90:114109

Vargaftik NB, Volkov BN, Voljak LD (1983) International tables of the surface-tension of water. J Phys Chem Ref Data 12(3):817–820

Xia YN, Whitesides GM (1998) Soft lithography. Angewandte Chemie-International Edition 37(5):551–575

Yu GR, Zhao DC, Wen L, Yang SD, Chen XC (2012) Viscosity of ionic liquids: database, observation, and quantitative structure-property relationship analysis. AICHE J 58(9):2885–2899